

SenseShift6D: Multimodal RGB-D Benchmarking for Robust 6D Pose Estimation across Environment and Sensor Variations

Yegyu Han¹, Taegyoon Yoon¹, Dayeon Woo¹, Sojeong Kim¹, and Hyung-Sin Kim¹

Graduate School of Data Science
Seoul National University
Seoul, Republic of Korea

{yegyuhan, taegyoun88, wuvel22, kvia2230, hyungkim}@snu.ac.kr

Abstract. Recent advances on 6D object pose estimation have achieved high performance on representative benchmarks such as LM-O, YCB-V, and T-Less. However, these datasets were captured under fixed illumination and camera settings, leaving the impact of real-world variations in illumination, exposure, gain or depth-sensor mode largely unexplored. To bridge this gap, we introduce *SenseShift6D*, the first RGB-D dataset that physically sweeps 13 RGB exposures, 9 RGB gains, auto-exposure, 4 depth-capture modes, and 5 illumination levels. For six common household objects, we acquire 198.8k RGB and 20.0k depth images (i.e., 795.4k RGB-D scenes), providing 1,380 unique sensor-lighting permutations per object pose. Experiments with state-of-the-art pretrained, generalizable pose estimators reveal substantial performance variation across lighting and sensor settings, despite their large-scale pretraining. Strikingly, even instance-level estimators—trained and tested on identical objects and backgrounds—exhibit pronounced sensitivity to environmental and sensor shifts. These findings establish sensor- and environment-aware robustness as an underexplored yet essential dimension for real-world deployment, and motivate *SenseShift6D* as a necessary benchmark for the community. Finally, to illustrate the opportunity enabled by this benchmark, we evaluate test-time multimodal sensor selection without retraining. An idealized (oracle) controller yields remarkable gains of up to +16.7 pp for generalizable models, whereas a practical consistency-based proxy improves performance only marginally, highlighting substantial headroom and the need for future research on reliable sensor-aware adaptation.

arXiv:2507.05751v3 [cs.CV] 19 Mar 2026

1 Introduction

Estimating the 6D pose of everyday objects is a critical computer vision task, enabling fine-grained interactions in mixed-reality headsets, autonomous-vehicle manipulation, and embodied AI agents navigating cluttered environments [7, 18, 28, 30, 34, 36]. The field has made substantial progress, with state-of-the-art methods achieving high accuracy on established benchmarks [3, 11–13, 17], including increasingly strong performance on challenging settings such as unseen objects and complex backgrounds.

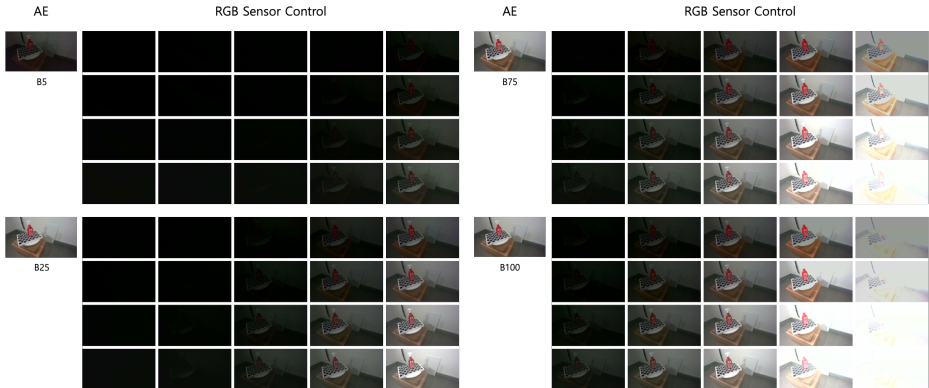


Fig. 1: RGB sample images under auto exposure and under all combinations of exposure and gain settings for brightness 5%, 25%, 75% and 100%. Rows indicate gain levels and columns indicate exposure levels.

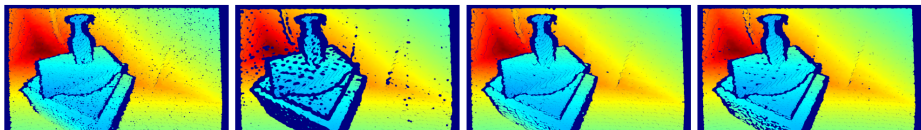


Fig. 2: Depth sample images under four depth capture modes: default, high accuracy, high density, and medium density.

Despite this progress, real deployments **rarely match** benchmark acquisition conditions. In practice, ambient illumination changes throughout the day; camera exposure and gain are adjusted by on-board auto-control or user settings; and commodity depth sensors switch capture modes on purpose. These environmental and sensor dynamics introduce complex artifacts—nonlinear color shifts, saturation, and structured depth noise—that are difficult to reproduce via synthetic augmentations or correct reliably in post-processing [2]. However, most widely used benchmarks are collected under **fixed** illumination and sensor configurations, leaving a key axis of robustness largely unmeasured: *how sensitive are 6D pose estimators to changes in illumination and camera/depth-sensor settings, even when the scene itself is simple?* While robustness to these covariate shifts have been recently studied in image classification tasks [1, 2, 19], the 6D pose community lacks a benchmark that systematically sweeps multimodal sensor parameters while providing accurate 6D ground truth. Without such a benchmark, it is difficult to compare methods fairly, diagnose failure modes, or develop principled solutions for environment- and sensor-aware robustness.

To bridge this gap, we introduce *SenseShift6D*, a novel RGB-D benchmark for 6D pose estimation that **physically sweeps key sensor and lighting parameters**. Using an Intel RealSense RGB-D camera in a controlled darkroom setup, we systematically vary 13 exposure levels, 9 gain settings, 4 depth-capture modes, and 5 illumination conditions across six representative household objects: a spray bottle, a Pringles tube, a tincase, a sandwich replica, a vertical mouse, and a rubber duck. This protocol produces 198.8k RGB and 20.0k depth frames,

which can provide 1,380 unique sensor-lighting permutations per object pose (Figs. 1 and 2), and 795.4k paired RGB-D scenes—to our knowledge, **the largest** of its kind ($\sim 6\times$ larger than the second largest 6D pose dataset [35]). Each scene is annotated with 6D poses via ChArUco calibration and manual refinement (with ~ 2 mm errors). We further define standardized splits: **Train-Def**, captured under default camera and illumination settings, and **Train-Var**, covering a comprehensive multimodal parameter grid. Correspondingly, we construct two test splits (**Test-Def** and **Test-Var**) without overlap with the training configurations. As all variations are physically realized, the captured images preserve authentic sensor artifacts, including nonlinear color shifts, photon-shot noise, and structured depth errors, that synthetic augmentations cannot replicate.

Using *SenseShift6D*, we provide the first systematic characterization of this environmental- and sensor-shift axis across both (i) pretrained, generalizable pose estimators and (ii) instance-level models trained on the same objects. We find that performance can change substantially across illumination and sensor settings—even for single-object scenes with clean backgrounds—indicating that sensor/environment shifts constitute an **orthogonal and underexplored challenge** not covered by existing benchmarks or large-scale pretraining alone. This establishes sensor-aware evaluation as a necessary complement to the community’s current emphasis on clutter, occlusion, and category generalization. *SenseShift6D* also enables research on **sensor-aware inference**, including parameter selection at test time. In this work, we include simple sensor-selection baselines and oracle upper bounds as diagnostic tools. Oracle selection reveals substantial headroom: single-modal control is *already* effective (e.g., +9.4 percentage points (pp) on pretrained models), and **multimodal control** yields further improvements (e.g., +16.7 pp on the same models). However, a realistic consistency-proxy yields marginal gains. This clear gap underscores the need for future research on reliable sensor-aware adaptation, but our focus here is the benchmark and evaluation protocol that make such progress measurable and comparable.

This paper offers three main contributions:

- ***SenseShift6D* benchmark:** We present the first 6D object-pose benchmark that systematically and physically varies multimodal sensor parameters and illumination, with accurate 6D ground truth and standardized train/test splits.
- **A new robustness axis for 6D pose:** We reveal that illumination and sensor settings constitute an orthogonal axis of generalization. Both pretrained generalizable models and instance-level models degrade markedly under these shifts, even in low-complexity scenes.
- **Sensor-aware evaluation protocol and baselines:** We provide a structured evaluation suite and sensor-selection diagnostics (upper bounds and realistic proxies) to quantify robustness and headroom, enabling principled future work on sensor-aware 6D pose estimation.

By providing a structured testbed for sensor-aware object 6D pose estimation, *SenseShift6D* lays the groundwork for more robust, adaptive perception systems in dynamic real-world environments.

Table 1: Comparison of 6D pose estimation datasets in terms of sensor and lighting variation.

Dataset	Environmental and sensor variations					Objects	RGB	Depth	RGB-D
	Illumination	Exposure	Gain	Depth	Total Var.				
LM [11]	×	×	×	×	×	15	18.2k	18.2k	18.2k
LM-O [3]	×	×	×	×	×	8	1.2k	1.2k	1.2k
T-LESS [12]	×	×	×	×	×	30	49k	49k	49k
YCB-V [35]	×	×	×	×	×	21	133k	133k	133k
TUD-L [13]	8 options	×	×	×	8	3	62k	62k	62k
HB [17]	2 options	×	×	×	2	33	34.8k	34.8k	34.8k
HOPE [31]	5 options	×	×	×	5	28	238	238	238
IPD [16]	3 options	4 levels	×	×	12	20	30k	30k	30k
SenseShift6D (Ours)	5 levels	13 levels	9 levels	4 modes	1,380	6	198.8k	20.0k	795.4k

2 Related Work

2.1 6D Pose Estimation Benchmark

Classic datasets. LineMOD (LM) [11] and its occlusion subset (LM-O) [3] pioneered RGB-D pose estimation benchmarks in controlled tabletop setups. Subsequent benchmarks such as T-LESS [12], which provided a large collection of texture-less industrial objects, and YCB-V [35], which offered cluttered scenes with temporal sequences, expanded the scope of evaluation. While these benchmarks provide robust evaluation regarding variations in objects and their poses, all were captured under fixed illumination and camera settings.

Initial exploration of environmental and sensor variation. TUD-L [13], HomebrewedDB (HB) [17], and HOPE [31] introduced variations in illumination conditions but retained fixed camera settings with auto-exposure enabled. The recent Industrial Parts Dataset (IPD) [16] was the first benchmark to vary camera parameters, capturing four exposure levels under multiple lighting conditions. However, IPD focuses on texture-less industrial parts and does not explore variations in RGB gain or depth-sensor modes, thus limiting its suitability for adaptive-sensing research.

Remaining gap and our contribution. As summarized in Tab. 1, no existing benchmark offers orthogonal sweeps of RGB exposure, RGB gain, and multiple depth-capture modes together with dense 6D ground truth. Our *SenseShift6D* dataset directly addresses this gap by systematically varying exposure, gain, and depth-capture modes under diverse illumination conditions, enabling fine-grained analysis of 6D pose estimation robustness to realistic hardware-level changes.

2.2 Adaptive Sensor Control Benchmark

Prior studies [9, 27] have explored test-time adaptation of camera parameters to improve downstream vision performance, but these studies lacked explicit benchmarks in real-world. Recently, ImageNet-ES [2] and ImageNet-ES-Diverse [1] captured real-world scenes using a *physical* camera, systematically varying aperture, shutter speed, and ISO across multiple lighting conditions for image classification tasks. These benchmarks demonstrated that physical variation *cannot be*

Table 2: SenseShift6D Configurations for Data split. Auto images for each split are processed from multiple auto-exposure shots.

Data split	Brightness (%)	Sensor configuration	Exposure (μ s)	Gain	Depth-capture mode	Captured images
Train-Def	50	Auto (1 RGB options, 1 depth option)	Auto	Auto	Default	RGB: 750, Depth: 750 1 RGB-D scene/pose
Train-Var	5, 25, 50, 75, 100	Auto + Manual (41 RGB options, 1 depth options)	Auto, 2, 4, 19, 78, 312, 1250, 5000, 10000	Auto, 0, 32, 64, 96, 128	Default	RGB: 153.7k, Depth: 3.7k 205 RGB-D scenes/pose
Test-Def	50	Auto (1 RGB option, 1 depth option)	Auto	Auto	Default	RGB: 251, Depth: 251 1 RGB-D scenes/pose
Test-Var	5, 25, 50, 75, 100	Auto + Manual (21 RGB options, 4 Depth options)	Auto, 9, 39, 156, 625, 2500	Auto, 16, 48, 80, 112	Default, High Accuracy, High Density, Medium Density	RGB: 26.3k, Depth: 5.0k 420 RGB-D scenes/pose

replicated by synthetic augmentations and dynamically selecting optimal camera parameters at test time can significantly increase the performance of lightweight models, enabling accuracy competitive with larger foundation models without additional training.

However, existing adaptive sensing research remains limited to single-modal RGB classification. To date, no prior work has explored: (1) multimodal sensor control, where depth-sensor modes must be jointly optimized with RGB settings; or (2) the impact of adaptive sensor control on object-centric 6D pose estimation tasks, which inherently rely on both photometric and geometric cues. Our *SenseShift6D* addresses this gap by providing the first realistic testbed for evaluating multimodal, per-frame sensor-control policies alongside conventional data-centric training baselines.

3 SenseShift6D

We introduce *SenseShift6D*, the first RGB-D benchmark that *physically* sweeps camera and lighting parameters, enabling rigorous evaluation of 6D object pose estimators under realistic environmental and sensor dynamics. Using an Intel RealSense D455 mounted in a darkroom, we systematically capture six representative household objects—spray, Pringles, tincase, sandwich, mouse, and duck—selected to reflect diverse combinations of RGB and geometric features (Fig. 3), under auto-exposure, 13 RGB-exposure times, 9 RGB-gain settings, 4 depth-capture presets, and 5 illumination levels (details in Tab. 2). Our dataset contains 198.8k RGB and 20.0k depth frames, resulting in 1,380 unique sensor-lighting configurations per object pose (i.e., 5 brightness level \times 4 depth modes \times (45 RGB for training + 24 RGB for testing)) and 795.4k RGB-D scene instances (i.e., 5 brightness level \times 4 depth modes \times (750 object poses \times 45 RGB for training + 251 object poses \times 24 RGB for testing)), the *largest* among the current benchmarks to our knowledge. Accurate ground truth is obtained via a rigidly mounted ChArUco board and careful hand-eye calibration.

**Fig. 3: Six household objects collected in SenseShift6D.**

To facilitate controlled benchmarking, we organize the dataset into four clearly defined splits:

- **Train-Def:** Contains only the default sensor and lighting configuration (1 RGB-D scene/pose)
- **Train-Var:** Expands Train-Def, covering $(8 \text{ exposures} \times 5 \text{ gains} + 1 \text{ auto-exposure}) \times 1 \text{ depth mode} \times 5 \text{ brightness levels}$ (205 RGB-D scenes/pose).
- **Test-Def:** Includes the default sensor and lighting configuration (1 RGB-D scene/pose)
- **Test-Var:** Expands Test-Def, featuring $(5 \text{ exposures} \times 4 \text{ gains} + 1 \text{ auto-exposure}) \times 4 \text{ depth-modes} \times 5 \text{ brightness levels}$ (420 RGB-D scenes/pose).

As all variations are physically captured rather than digitally simulated, the resulting images inherently retain authentic artifacts, such as non-linear color shifts, photon-shot noise, and depth-mode-specific errors, that synthetic augmentation methods cannot reproduce [2]. *SenseShift6D* therefore offers the first realistic testbed for analyzing environment- and sensor-aware robustness, enabling side-by-side evaluation of per-frame adaptive-sensing policies against traditional data-centric training strategies.

3.1 Environmental and Sensor Variations

Ambient-illumination sweep. Real deployments frequently encounter lighting changes, such as those found in warehouse aisles, outdoor loading bays, or dim domestic environments. To reproduce these diverse conditions in a controlled manner, we built a darkroom enclosed with black curtains to block external light completely. Within this setup, we installed three Philips Hue White & Color Ambiance bulbs, providing precise and programmable brightness control. Each bulb was calibrated to a consistent color temperature of 6535 K, with brightness systematically varied across five levels: 5%, 25%, 50%, 75% and 100%. This controlled setting ensures uniform illumination conditions, enabling accurate comparisons of RGB gain and exposure settings under identical photon flux.

RGB-sensor parameters. Most RGB cameras permit manual control of two key RGB sensor parameters: exposure, determining the duration of sensor exposure to incoming light, and gain, which amplifies the captured signal strength.

- **Exposure grid.** The camera supports exposure values ranging from $1 \mu\text{s}$ to $10,000 \mu\text{s}$. Empirical tests indicated that exposure times below $1,000 \mu\text{s}$ yield image quality comparable to the camera’s auto-exposure setting in well-lit environments. Given that this threshold is relatively low within the configurable range, we chose 13 logarithmically spaced exposure values to maximize coverage across practical operating conditions.
- **Gain grid.** The RGB gain of the camera can be ranges from 0 to 128. Through visual inspection, we found that linear steps produce more diverse characteristics than exponential spacing. Therefore, we selected 9 linearly spaced gain settings spanning the full range.

Depth capture modes. Depth maps are generated via stereo matching, estimating depth by aligning left and right camera images. To control the depth sensing behavior, we leverage four predefined depth presets provided by Intel, each optimized for different density–accuracy characteristics [14]:

- **Default:** Offers visually clean depth maps with reduced noise and well-defined edges, suitable for general-purpose applications.
- **High Accuracy:** Provides highly reliable depth estimates by enforcing stricter confidence thresholds, albeit at the expense of a lower fill rate.
- **High Density:** Increases the fill factor, providing more complete depth maps, particularly effective for detecting more surfaces in low-texture areas.
- **Medium Density:** Offers a balanced trade-off between fill factor and accuracy, aiming to balance depth map completeness and precision.

3.2 Dataset Collection

To capture each scene systematically, we acquired images under all sensor configurations associated with a given data split, while maintaining fixed positions for the object and camera. Scenes were assigned exclusively to specific splits, ensuring that poses and RGB sensor configurations do not overlap between training and test sets. To capture diverse object poses, we used a motorized turntable to vary object orientation and adjusted the camera’s position and tilt angle. Each object was rigidly mounted onto a ChArUco board, which was firmly placed on the turntable, providing a consistent and precise pose reference throughout data capture.

For automatic collection, the turntable was remotely controlled, and deliberate delays were introduced after changing lighting brightness or sensor parameters, allowing sufficient stabilization time. We employed one smart IR remote-control hub to send commands to the turntable and another hub to control three smart bulbs. Both hubs received commands from a cloud-based server, which coordinated the entire data-capture sequence through an integrated control script (see Fig. 4).

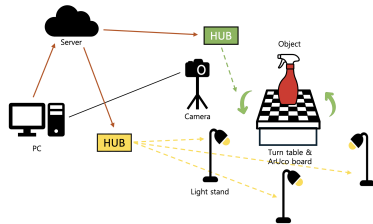


Fig. 4: Testbed for data collection.

Table 3: GT annotation accuracy (mm).

	μ_δ	σ_δ	$\mu_{ \delta }$	$med_{ \delta }$
RealSense	-0.28	3.29	2.32	1.73

3.3 Data Processing

Validation. We manually reviewed the images for each parameter configuration. If any scene appeared inconsistent due to lighting or sensor parameter change delays, we excluded that scene across all configurations to maintain dataset consistency.

Stabilizing auto-exposure frames. The default setting to capture RGB images is the auto-exposure mode. For the D455 camera, we observed that the auto-exposure setting depends on the gain value set in the previous frame, leading to frame-to-frame brightness jitter. To suppress this effect, we captured successive auto-exposure shots of each scene (5 shots for Train-Def/Var and 4 shots for Test-Def/Var), each preceded by a different gain initialization, and averaged them to obtain a stable reference image.

Ground-Truth annotation. For each pose, we used the 50%-brightness, averaged auto-exposure RGB frame and went through the annotation process below, resulting in about 2 mm errors.

- **Object masks:** Initially, rough bounding boxes were generated using Grounding DINO [23], guided by shape-aware textual prompts tailored to each object. Boxes were manually reviewed and corrected if needed. The refined boxes were passed to FastSAM [37] to generate precise instance-level masks.
- **Accuracy of GT annotation:** Following the protocol in [12, 17], we calculate the difference $\delta = d_c - d_r$, where d_c denotes the captured depth map and d_r denotes the rendered depth map using the GT pose. Differences over 5 cm are treated as outliers and omitted. Tab. 3 reports the mean μ_δ , standard deviation σ_δ , and the mean and median of the absolute differences $\mu_{|\delta|}$ and $med_{|\delta|}$. High-accuracy depth sensing is employed for reliable evaluation of GT accuracy analysis.

4 Experiments

Goal. *SenseShift6D* is designed to isolate an under-measured robustness axis—illumination and sensor-setting variation—and to make its effects measurable across 6D pose estimation pipelines. Accordingly, our experiments quantify (i) how much accuracy varies under these shifts, and (ii) the headroom available if one could select sensor settings effectively at test time (used here as diagnostic upper bounds, not as a proposed control method).

Models. To quantify the effect of illumination and sensor variations—and the gains from sensor adaptation—relative to conventional training–inference paradigms (large-scale pretraining and standard supervised pipelines), we evaluate several state-of-the-art methods:

- **Pretrained, generalizable models (unseen objects; RGB-D):** **GigaPose** [26], **SAM-6D** [21], and **FoundationPose** [33]. GigaPose and SAM-6D were pretrained on the large-scale MegaPose [20], which contains objects from ShapeNet [4] and GSO [8]. FoundationPose uses a custom data-generation pipeline with 3D assets from GSO and Objaverse [5].
- **Instance-level models (known objects):** **ZebraPose** [29], an RGB-based method with a ResNet-34 backbone; **GDRNPP** [24], which builds on GDRNet [32] using a ConvNeXt [25] backbone and depth-based refinement module; and **HiPose** [22], an RGB-D approach that fuses ConvNeXt-based RGB features with RandLA-Net [15] depth features. These models are trained on *SenseShift6D*.

Sensor-setting evaluation protocols (diagnostics). To characterize sensitivity and headroom, we report five regimes: (1) **Baseline:** default settings for both RGB (e.g., auto-exposure) and depth sensors; (2) **Depth-Only (oracle):** per-scene best depth preset among the available modes and default auto-exposure for RGB; (3) **RGB-Only (oracle):** per-scene best exposure/gain, keeping depth default; (4) **Oracle-Fixed:** a single globally best RGB-D configuration applied to all test scenes; (5) **Oracle-Dynamic:** per-scene best joint RGB-D configuration.

Table 4: AUC@[0:0.1] performance of various sensor control methods for unseen object pose estimation models: GigaPose, SAM-6D, FoundationPose.

Model	Object	Baseline	Depth-Only	RGB-Only	Oracle-Fixed	Oracle-Dynamic
		RGB: Auto Depth: Default	RGB: Auto Depth: Oracle	RGB: Oracle Depth: Default	Best Fixed Param.	RGB: Oracle Depth: Oracle
GigaPose [26]	Spray	63.94	72.41 (+8.47)	76.42 (+12.48)	67.98 (+4.03)	81.24 (+17.30)
	Pringles	20.91	46.74 (+25.83)	46.13 (+25.22)	30.82 (+9.90)	70.54 (+49.63)
	Tincase	64.49	72.67 (+8.18)	69.32 (+4.84)	65.51 (+1.02)	76.41 (+11.92)
	Sandwich	64.94	71.92 (+6.98)	76.09 (+11.14)	67.90 (+2.96)	83.88 (+18.94)
	Mouse	56.62	67.40 (+10.79)	67.02 (+10.40)	53.46 (-3.16)	76.71 (+20.09)
	Duck	72.26	78.72 (+6.46)	77.67 (+5.40)	71.83 (-0.43)	82.62 (+10.36)
	Overall	57.19	68.31 (+11.12)	68.77 (+11.58)	59.58 (+2.39)	78.57 (+21.38)
SAM-6D [21]	Spray	83.14	85.62 (+2.48)	82.64 (-0.50)	83.34 (+0.20)	88.50 (+5.36)
	Pringles	64.09	73.96 (+9.87)	74.07 (+9.98)	64.54 (+0.45)	80.63 (+16.54)
	Tincase	73.42	77.53 (+4.11)	80.19 (+6.77)	68.95 (-4.47)	83.32 (+9.90)
	Sandwich	78.39	78.99 (+0.60)	80.02 (+1.63)	78.38 (-0.02)	80.81 (+2.41)
	Mouse	55.72	62.25 (+6.53)	67.69 (+11.96)	58.63 (+2.91)	72.45 (+16.72)
	Duck	76.67	82.42 (+5.74)	83.40 (+6.72)	78.58 (+1.90)	87.64 (+10.97)
	Overall	71.91	76.80 (+4.89)	78.00 (+6.09)	72.07 (+0.16)	82.22 (+10.32)
FoundationPose [33]	Spray	84.63	86.52 (+ 1.89)	87.60 (+2.97)	83.96 (-0.67)	89.01 (+4.38)
	Pringles	34.26	50.72 (+16.46)	50.78 (+16.52)	37.73 (+3.47)	74.69 (+40.43)
	Tincase	38.24	56.16 (+17.92)	69.38 (+31.14)	40.07 (+1.83)	82.79 (+44.55)
	Sandwich	83.17	86.40 (+3.23)	85.12 (+1.95)	83.14 (-0.03)	88.11 (+4.94)
	Mouse	70.22	74.34 (+4.12)	75.86 (+5.64)	70.69 (+0.46)	79.98 (+9.75)
	Duck	84.78	86.87 (+2.09)	89.15 (+4.37)	84.72 (-0.06)	90.67 (+5.89)
	Overall	65.88	73.50 (+7.62)	76.32 (+10.43)	66.72 (+0.83)	84.21 (+18.32)

Here, ‘‘Oracle’’ represents an *offline upper bound* obtained by evaluating the full sensor-configuration grid and marking a scene correct if *any* configuration yields a correct pose. This is used to quantify *headroom*, not as a deployable policy.

Metrics. We use the standard Average Distance (ADD) metric [11], which measures the average point-wise distance between model points transformed by the predicted pose and the ground-truth pose. Based on this metric, we report two evaluation measures: **AUC@[0:0.1]**, which corresponds to the area under the ADD recall curve up to a threshold of 10% of the object diameter, and **AR@5**, which denotes the recall at a threshold of 5% of the object diameter. Due to space limits, additional metrics—average recall of VSD, MSSD and MSPD [13]—are reported in Appendix Sec. D.

4.1 Analysis on Pretrained, Generalizable Pose Estimation Models

Generalizable 6D pose estimators are designed to cope with clutter, occlusion, and novel objects by leveraging large-scale pretraining. *SenseShift6D* intentionally removes these confounders—single object, clean background, no occlusion—so that evaluation isolates robustness to **environmental and sensor shifts**. We therefore test whether robustness learned from pretraining transfers to this *orthogonal and underexplored axis*: variations in illumination and RGB/depth sensor parameters that are largely absent from existing benchmarks.

Tab. 4 presents the impact of illumination and sensor variations on 6D pose estimation, evaluated with ground-truth object segmentations. Since SAM-6D includes its own image segmentation model (ISM), while GigaPose and

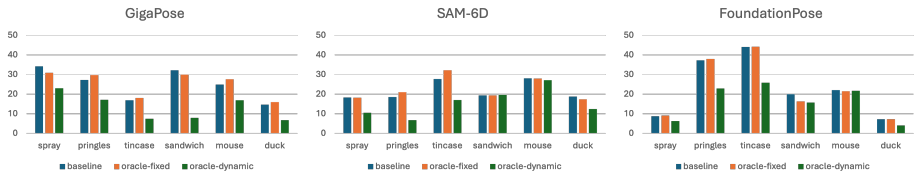


Fig. 5: Overall standard deviation of AUC computed across all brightness and scenes evaluated under Baseline, Oracle-Fixed, Oracle-Dynamic.

FoundationPose assume object masks are given, we also provide the results of SAM-6D’s full pipeline in Appendix Sec. C for completeness.

Sensitivity under default sensing. Under Baseline (auto-exposure RGB + Default depth), all pretrained models exhibit significant performance drop. This confirms that, even with strong pretraining, robustness does not automatically extend to sensor- and illumination-induced shifts.

Headroom diagnostics via oracle selection. Oracle regimes reveal substantial headroom of test-time sensor control without model retraining. On average across the three pretrained models, RGB-Only improves AUC by +9.4 pp and Depth-Only by +7.9 pp over Baseline, indicating that factory defaults are not model-optimal. Furthermore, joint multimodal selection (Oracle-Dynamic) achieves the best results, with +16.7 pp over Baseline and +7.3 pp over the second-best RGB-Only. This gap indicates that RGB and depth provide *complementary cues* and that their optimal settings can interact non-trivially.

The full-pipelined SAM-6D (Appendix Tab. 9) exhibits a relatively lower baseline due to the absence of ground-truth masks; conversely, since sensor configurations also affect segmentation, oracle selection yields more substantial performance gains.

Limitation of fixed tuning. In contrast, Oracle-Fixed provides only +1.1 pp on average—and can even underperform Baseline (e.g., SAM-6D on Tincase in Tab. 4). This is a clean benchmark finding: there is no single sensor configuration that generalizes across lighting and object appearances, motivating evaluation—and eventually methods—that are **scene-adaptive** rather than globally tuned.

Stability and object-wise disparity. *SenseShift6D* also exposes large object-wise performance gaps under Baseline: the average gap between the best- and worst-performing objects is 43.1 pp, which shrinks to 15.1 pp under Oracle-Dynamic. Moreover, Fig. 5 shows that per-scene oracle selection reduces *scene-level variability* under the same object. The overall AUC standard deviation decreases by 8.4 pp relative to Baseline, with GigaPose on the Sandwich showing the largest reduction of 24.3 pp.

Together, these results show that sensor/illumination shifts are a distinct robustness axis that remains challenging even for pretrained generalizable pose estimators. Qualitative examples are provided in Appendix Sec. F.1.

4.2 Analysis on Instance-Level Pose Estimation Models

Instance-level methods follow the standard train–test setup in which the training and test sets share the same object domain. Building on Sec. 4.1, our goal

Table 5: AR@5 performance of various sensor control methods under different training and test settings of *SenseShift6D* for instance-level pose estimation models: ZebraPose, GDRNPP, HiPose.

Object	Train	ZebraPose [29]			GDRNPP [24]			HiPose [22]					
		Test-Def	Test-Var	Oracle	Test-Def	Test-Var	Oracle	Test-Def	Test-Var	Oracle			
Spray	PBR + Train-Def	100.0	96.10	54.61	98.54	100.0	96.59	52.02	99.02	100.0	99.51	59.88	100.0
	PBR + Train-Def w/ Aug	95.12	93.66	64.98	99.51	100.0	98.54	71.88	100.0	100.0	100.0	89.76	100.0
	PBR + Train-Var	97.56	97.07	79.24	97.56	97.56	97.56	85.93	98.54	100.0	100.0	100.0	100.0
Pringles	PBR + Train-Def	90.48	84.29	43.31	95.71	69.05	60.95	35.64	89.05	100.0	99.52	58.71	100.0
	PBR + Train-Def w/ Aug	64.29	64.76	44.38	93.33	80.95	79.05	49.17	89.52	97.62	97.62	72.95	100.0
	PBR + Train-Var	83.33	82.38	64.86	90.95	90.48	90.00	72.21	97.14	97.62	97.62	86.88	98.10
Tincase	PBR + Train-Def	97.78	86.67	45.78	96.44	91.11	81.33	46.56	92.89	97.78	86.67	53.62	96.44
	PBR + Train-Def w/ Aug	97.78	94.67	59.38	100.0	82.22	82.22	55.78	95.11	97.78	96.89	86.62	97.78
	PBR + Train-Var	97.78	98.22	75.09	100.0	100.0	99.56	82.00	100.0	97.78	97.78	97.76	97.78
Sandwich	PBR + Train-Def	94.87	89.23	48.38	99.49	97.44	88.21	47.03	96.41	94.87	92.87	57.21	94.87
	PBR + Train-Def w/ Aug	92.31	88.72	57.82	99.49	94.87	92.31	63.72	98.97	94.87	94.36	84.46	94.87
	PBR + Train-Var	92.31	90.77	67.03	96.41	97.44	97.44	82.64	100.0	94.87	94.87	94.87	94.87
Mouse	PBR + Train-Def	70.73	62.44	27.00	87.80	95.12	76.10	31.44	88.78	90.24	79.02	43.68	87.80
	PBR + Train-Def w/ Aug	48.78	48.78	32.46	87.80	78.05	72.68	43.29	86.83	90.24	90.24	82.44	90.73
	PBR + Train-Var	46.34	47.80	35.07	71.22	80.49	80.49	66.39	91.22	90.24	90.24	87.29	90.73
Duck	PBR + Train-Def	93.02	84.19	28.95	94.88	95.35	84.65	39.63	99.07	97.67	80.00	44.56	99.53
	PBR + Train-Def w/ Aug	93.02	84.65	54.63	98.60	90.70	84.65	57.91	99.07	97.67	98.60	82.86	100.0
	PBR + Train-Var	93.02	93.02	71.77	98.60	97.67	97.67	81.44	99.53	97.67	98.60	97.49	100.0
Overall	PBR + Train-Def	91.15	83.82	41.34	95.48	91.34	81.30	42.05	94.20	96.76	89.59	52.94	96.44
	PBR + Train-Def w/ Aug	81.88	79.21	52.27	96.46	87.80	84.91	56.96	94.92	96.36	96.29	83.18	97.23
	PBR + Train-Var	85.06	84.88	65.51	92.46	93.94	93.79	78.44	97.74	96.36	96.52	94.05	96.91

here is twofold: (i) to test whether environmental and sensor variations remain challenging once the unseen-object factor is removed, and (ii) to assess whether adapting sensor configuration at test time remains effective even when the training data already includes various augmentations or explicit physical sensor and illumination variation.

For training, we generated 10k photorealistic (PBR) synthetic images per object using BlenderProc [6]. Each model was trained independently on a per-object basis under three schemes: (1) **PBR + Train-Def** (default physical images only), (2) **PBR + Train-Def with augmentation** (including Gaussian blur, linear contrast adjustment, brightness enhancement and others; see Appendix Sec. A.), and (3) **PBR + Train-Var** (full sensor and lighting variation). In all experiments, we excluded refinement modules for ZebraPose and GDRNPP, and used the full pipeline for HiPose. Since HiPose is the only RGB-D method (ZebraPose and GDRNPP are RGB-only), we report results in two parts.

Tab. 5 evaluates the impact of illumination and RGB sensor variations (with the default depth preset) under three sensor-control settings: **Auto** (auto-exposure), **Rand** (average performance across randomly selected exposure-gain pairs), and **Oracle** (per-scene upper bound over the full RGB grid). Tab. 6 evaluates HiPose (training scheme 1) on Test-Var under the multimodal regimes introduced in Sec. 4.1.

RGB/illumination shift remains a challenge, even for known objects. Tab. 5 (default depth preset) shows that when trained with Train-Def, Auto performance consistently drops from Test-Def to Test-Var (e.g., overall -7.3 pp

Table 6: AUC@[0:0.1] performance of various sensor control methods for HiPose, trained on PBR + Train-Def and tested on Test-Var.

Object	Baseline	Depth-Only	RGB-Only	Oracle-Fixed Best Fixed Param.	Oracle-Dynamic
	RGB: Auto Depth: Default	RGB: Auto Depth: Oracle	RGB: Oracle Depth: Default		RGB: Oracle Depth: Oracle
Spray	86.92	88.17 (+1.25)	88.79 (+1.87)	71.70 (-15.22)	89.87 (+2.95)
Pringles	73.40	76.18 (+2.78)	79.08 (+5.68)	64.23 (-9.16)	81.55 (+8.15)
Tincase	74.78	77.88 (+3.10)	85.30 (+10.52)	67.52 (-7.27)	86.84 (+12.06)
Sandwich	78.68	81.72 (+3.04)	84.06 (+5.38)	66.19 (-12.48)	86.43 (+7.75)
Mouse	63.92	66.41 (+2.49)	72.19 (+8.27)	53.25 (-10.67)	75.21 (+11.29)
Duck	70.27	72.94 (+2.67)	86.67 (+16.40)	65.54 (-4.73)	88.46 (+18.19)
Overall	74.66	77.22 (+2.44)	82.68 (+8.02)	64.74 (-9.92)	84.73 (+10.07)

for ZebraPose, -10.0 pp for GDRNPP, -7.2 pp for HiPose), confirming that sensor/illumination shifts is impactful even with identical objects and backgrounds. Oracle selection (RGB) substantially closes this gap: Oracle on Test-Var consistently outperforms Auto on Test-Var and often matches or exceeds Auto on Test-Def, indicating that a significant portion of the failure is attributable to **capture conditions that suppress or corrupt informative cues**.

Multimodal shifts for an instance-level RGB-D model. HiPose performance in Tab. 6 reveals that, while all test-time sensor-selection regimes improve over Baseline, the average gain from RGB-Only (+8.02 AUC) is substantially larger than that from Depth-Only (+2.44 AUC), unlike the pretrained setting where both modalities often contribute strongly (Tab. 4). This is expected because HiPose is trained instance-level with depth maps from the same domain as the Baseline depth preset, and depth is generally less sensitive to illumination changes than RGB. Importantly, depth-mode selection still provides performance gains, and joint per-scene selection remains best overall (Oracle-Dynamic: +10.07 AUC), indicating that RGB and depth can still provide complementary robustness depending on the scene.

Data-centric robustness is helpful but incomplete. In Tab. 5, data augmentation generally improves Auto on Test-Var for GDRNPP/HiPose, but can hurt for some cases (e.g., Mouse for GDRNPP), indicating that synthetic perturbations are not uniformly reliable. Training on expanded physically captured variation (PBR + Train-Var, 3.5× larger than PBR + Train-Def) yields larger and more consistent gains than augmentation overall, underscoring *the value of real sensor variation*. However, it can still fail in difficult regimes (e.g., Mouse for ZebraPose), suggesting that “more diverse training data” is not a guaranteed solution when the sensing process itself removes critical cues.

Sensor-aware diagnostics vs. scaling data. An important benchmark finding is that oracle selection with limited training can rival or exceed data-scaling baselines: for example, ZebraPose trained on Train-Def with Oracle achieves >+10 pp higher accuracy on Test-Var than Auto trained on Train-Var (Tab. 5). This highlights the benchmark’s core message: robustness under sensor/environment shifts is not only a modeling problem, but also a sensing problem—capturing

Table 7: Performance comparison under different sensor selection strategies. Values in parentheses denote ADD-S variant. Supervised models are trained under the PBR + Train-Def setting.

(a) Supervised Models (AR@5)					(b) Pretrained Models (AUC@[0:0.1])			
Model	Test-Def		Test-Var		Model	Baseline	Oracle	Proxy
	Auto	Auto	Oracle	Proxy				
ZebraPose [29]	91.15 (93.10)	83.82 (87.83)	95.48 (96.79)	91.23 (93.82)	GigaPose [26]	57.19 (68.64)	78.57 (83.62)	59.32 (77.41)
GDRNPP [24]	91.34 (97.19)	81.30 (88.77)	94.20 (96.75)	90.76 (93.54)	SAM-6D [21]	71.91 (78.12)	82.22 (84.78)	64.88 (80.72)
HiPose [22]	96.76 (96.76)	89.59 (90.34)	97.19 (97.34)	96.95 (97.25)	FoundationPose [33]	65.88 (82.90)	84.21 (88.19)	62.82 (82.51)

more reliable observations can be as important as (or complementary to) scaling training data. Qualitative examples are provided in Appendix Sec. F.2.

4.3 Towards Online Sensor Adaptation (Proxy Baseline)

Oracle selection quantifies headroom but is not deployable, since ground truth (GT) is unavailable at test time. To ground future work, we evaluate a simple proxy-based baseline that attempts to pick sensor settings without GT (i.e., not a final solution but a practical baseline to quantify the gap to oracle).

Proxy design. We consider VSD (Visible Surface Discrepancy) [13] as a proxy for sensor selection at inference time. Since VSD captures the geometric consistency between the ground-truth and estimated poses, it provides a potential signal for assessing pose quality and guiding sensor adaptation. For each scene, we analyze the correlation between ADD and VSD across different sensor configurations. The results (Appendix Sec. H) show moderate-to-strong correlation (above 0.86 for supervised models, 0.62 for pretrained models).

With the motivation, we design a VSD-like proxy metric as follows:

$$\text{proxy}_{\text{VSD}}(\hat{S}, S_I, \hat{V}, V_I, \tau) = \text{avg}_{p \in \hat{V} \cap V_I} \begin{cases} 0, & \text{if } p \in \hat{V} \cap V_I \wedge |\hat{S}(p) - S_I(p)| < \tau, \\ 1, & \text{otherwise.} \end{cases} \quad (1)$$

Here \hat{S} and S_I denote the distance maps rendered from the estimated pose and computed from the observed depth map, respectively. V_I denotes the dataset-provided visible object mask, while \hat{V} is the estimated visibility mask obtained from (\hat{S}, S_I) . In addition, we compute the IoU between V_I and \hat{V} , and use it as a tie-breaking criterion to resolve ambiguous cases during sensor selection.

Results and remaining gap. Tab. 7 reports the performance when applying the proposed proxy-based sensor selection. For supervised/instance-level models on Test-Var (Tab. 7a), the proxy consistently improves over Auto and can approach the oracle ceiling in favorable cases (e.g., HiPose). However, for pretrained generalizable models (Tab. 7b), the proxy yields only marginal gains under ADD and can even underperform Baseline. The proxy’s performance significantly improves under ADD-S, suggesting that **symmetry and pose ambiguity** (and the proxy’s lack of RGB appearance cues) are key failure modes. Overall, this

experiment reinforces the benchmark’s motivation: *SenseShift6D* exposes large headroom, but achieving it in practice requires stronger, multimodal proxy signals and principled sensor-aware selection strategies.

5 Conclusion

We introduced *SenseShift6D*, a physically captured RGB-D benchmark that *systematically sweeps* illumination, RGB exposure/gain, and depth-capture presets to isolate the impact of environment and sensor shifts on 6D object pose estimation. *SenseShift6D* provides accurate 6D ground truth, standardized non-overlapping splits, and a dense grid of real sensor-induced artifacts (e.g., non-linear color shifts and depth-mode-specific distortions) that are difficult to reproduce with synthetic augmentation.

Using this benchmark, we establish **sensor/environment shift as a distinct robustness axis** that is not covered by existing pose benchmarks or by large-scale pretraining alone. Across three state-of-the-art pretrained, generalizable estimators (GigaPose, SAM-6D, FoundationPose) and three supervised instance-level estimators (ZebraPose, GDRNPP, HiPose), performance varies substantially with illumination and sensor settings even in single-object, uncluttered scenes. Moreover, under pretrained models, per-scene sensing adaptation (Oracle-Dynamic) reveals substantial headroom, improving accuracy by *on average* +16.7 pp over factory defaults, whereas a single globally fixed configuration (Oracle-Fixed) yields only marginal gains (and can even underperform the default). Beyond mean accuracy, per-scene adaptation also reduces object-wise disparity and scene-level variability, indicating improved *stability* in addition to higher accuracy. Finally, to illustrate the opportunities enabled by *SenseShift6D* (without claiming a complete solution), we benchmark simple sensor-selection baselines alongside oracle upper bounds. While an oracle controller quantifies large headroom, a practical consistency-based selection closes only a small fraction of the gap for pretrained models, highlighting the need for future research on reliable, model-aware selection signals that jointly leverage photometric and geometric cues and handle pose symmetries.

Limitations and Future Work. *SenseShift6D* currently focuses on single-object tabletop scenes with simple backgrounds and no occlusion, and varies illumination primarily through brightness magnitude (without directional lighting and cast shadows). In addition, using a visible ChArUco board for pose annotation may introduce visual artifacts not present in deployment (reported in Appendix Sec. E). Future versions will expand (i) **scene complexity** (multi-object scenes, occlusions, and diverse backgrounds), (ii) **illumination variation** (directionality, shadows, and mixed color temperatures), and (iii) **annotation strategies** that avoid visible markers. Beyond dataset growth, *SenseShift6D* motivates new algorithmic directions: reliable practical proxy, learning-based or bandit-style sensor-selection policies, multimodal selection criteria that combine RGB appearance with depth geometry, and real-time sensing frameworks that adapt capture settings online to maintain reliable observations for downstream pose estimation under covariate shift.

References

1. Baek, E., Han, S., Gong, T., Kim, H.S.: Adaptive camera sensor for vision models. In: The Thirteenth International Conference on Learning Representations (2025)
2. Baek, E., Park, K., Kim, J., Kim, H.S.: Unexplored faces of robustness and out-of-distribution: Covariate shifts in environment and sensor domains. In: Proceedings of the IEEE/CVF Conference on Computer Vision and Pattern Recognition. pp. 22294–22303 (2024)
3. Brachmann, E., Krull, A., Michel, F., Gumhold, S., Shotton, J., Rother, C.: Learning 6D object pose estimation using 3D object coordinates. In: European conference on computer vision. pp. 536–551. Springer (2014)
4. Chang, A.X., Funkhouser, T., Guibas, L., Hanrahan, P., Huang, Q., Li, Z., Savarese, S., Savva, M., Song, S., Su, H., et al.: ShapeNet: An information-rich 3D model repository. arXiv preprint arXiv:1512.03012 (2015)
5. Deitke, M., Schwenk, D., Salvador, J., Weihs, L., Michel, O., VanderBilt, E., Schmidt, L., Ehsani, K., Kembhavi, A., Farhadi, A.: Objaverse: A universe of annotated 3D objects. In: Proceedings of the IEEE/CVF conference on computer vision and pattern recognition. pp. 13142–13153 (2023)
6. Denninger, M., Winkelbauer, D., Sundermeyer, M., Boerdijk, W., Knauer, M., Strobl, K.H., Humt, M., Triebel, R.: BlenderProc2: A procedural pipeline for photorealistic rendering. *Journal of Open Source Software* **8**(82), 4901 (2023). <https://doi.org/10.21105/joss.04901>, <https://doi.org/10.21105/joss.04901>
7. Doughty, M., Ghugre, N.R.: HMD-EgoPose: Head-mounted display-based egocentric marker-less tool and hand pose estimation for augmented surgical guidance. *International journal of computer assisted radiology and surgery* **17**(12), 2253–2262 (2022)
8. Downs, L., Francis, A., Koenig, N., Kinman, B., Hickman, R., Reymann, K., McHugh, T.B., Vanhoucke, V.: Google Scanned Objects: A high-quality dataset of 3D scanned household items. In: 2022 International Conference on Robotics and Automation (ICRA). pp. 2553–2560. Ieee (2022)
9. Goudreault, F., Scheuble, D., Bijelic, M., Robidoux, N., Heide, F.: LiDAR-in-the-loop hyperparameter optimization. In: Proceedings of the IEEE/CVF Conference on Computer Vision and Pattern Recognition. pp. 13404–13414 (2023)
10. Govi, E., Sapienza, D., Scribano, C., Poppi, T., Franchini, G., Ardòn, P., Verucchi, M., Bertogna, M.: Uncovering the background-induced bias in RGB based 6-DoF object pose estimation. arXiv preprint arXiv:2304.08230 (2023)
11. Hinterstoisser, S., Lepetit, V., Ilic, S., Holzer, S., Bradski, G., Konolige, K., Navab, N.: Model based training, detection and pose estimation of texture-less 3D objects in heavily cluttered scenes. In: Asian conference on computer vision. pp. 548–562. Springer (2012)
12. Hodan, T., Haluza, P., Obdržálek, Š., Matas, J., Lourakis, M., Zabulis, X.: T-LESS: An RGB-D dataset for 6D pose estimation of texture-less objects. In: 2017 IEEE winter conference on applications of computer vision (WACV). pp. 880–888. IEEE (2017)
13. Hodan, T., Michel, F., Brachmann, E., Kehl, W., GlentBuch, A., Kraft, D., Drost, B., Vidal, J., Ihrke, S., Zabulis, X., et al.: BOP: Benchmark for 6D object pose estimation. In: Proceedings of the European conference on computer vision (ECCV). pp. 19–34 (2018)
14. Hsu, Y., Grunnet-Jepsen, A., Sweetser, J., Brook, S.: D400 series visual presets, <https://dev.realsenseai.com/docs/d400-series-visual-presets>, accessed: January 20, 2026

15. Hu, Q., Yang, B., Xie, L., Rosa, S., Guo, Y., Wang, Z., Trigoni, N., Markham, A.: RandLA-Net: Efficient semantic segmentation of large-scale point clouds. In: Proceedings of the IEEE/CVF conference on computer vision and pattern recognition. pp. 11108–11117 (2020)
16. Kalra, A., Stoppi, G., Marin, D., Taamazyan, V., Shandilya, A., Agarwal, R., Boykov, A., Chong, T.H., Stark, M.: Towards co-evaluation of cameras, HDR, and algorithms for industrial-grade 6DoF pose estimation. In: Proceedings of the IEEE/CVF Conference on Computer Vision and Pattern Recognition. pp. 22691–22701 (2024)
17. Kaskman, R., Zakharov, S., Shugurov, I., Ilic, S.: HomebrewedDB: RGB-D dataset for 6D pose estimation of 3D objects. In: Proceedings of the IEEE/CVF International Conference on Computer Vision Workshops. pp. 0–0 (2019)
18. Ke, L., Li, S., Sun, Y., Tai, Y.W., Tang, C.K.: GSNet: Joint vehicle pose and shape reconstruction with geometrical and scene-aware supervision. In: European Conference on Computer Vision. pp. 515–532. Springer (2020)
19. Kim, J.y., Baek, E., Kim, H.S.: ImageNet-sES: A first systematic study of sensor-environment simulation anchored by real recaptures. In: Proceedings of the IEEE/CVF Winter Conference on Applications of Computer Vision. pp. 1117–1126 (2026)
20. Labbé, Y., Manuelli, L., Mousavian, A., Tyree, S., Birchfield, S., Tremblay, J., Carpentier, J., Aubry, M., Fox, D., Sivic, J.: MegaPose: 6D pose estimation of novel objects via render & compare. In: Proceedings of the 6th Conference on Robot Learning (CoRL) (2022)
21. Lin, J., Liu, L., Lu, D., Jia, K.: SAM-6D: Segment anything model meets zero-shot 6D object pose estimation. In: Proceedings of the IEEE/CVF Conference on Computer Vision and Pattern Recognition. pp. 27906–27916 (2024)
22. Lin, Y., Su, Y., Nathan, P., Inuganti, S., Di, Y., Sundermeyer, M., Manhardt, F., Stricker, D., Rambach, J., Zhang, Y.: HiPose: Hierarchical binary surface encoding and correspondence pruning for RGB-D 6DoF object pose estimation. In: Proceedings of the IEEE/CVF Conference on Computer Vision and Pattern Recognition. pp. 10148–10158 (2024)
23. Liu, S., Zeng, Z., Ren, T., Li, F., Zhang, H., Yang, J., Jiang, Q., Li, C., Yang, J., Su, H., et al.: Grounding DINO: Marrying DINO with grounded pre-training for open-set object detection. In: European conference on computer vision. pp. 38–55. Springer (2024)
24. Liu, X., Zhang, R., Zhang, C., Wang, G., Tang, J., Li, Z., Ji, X.: GDRNPP: A geometry-guided and fully learning-based object pose estimator. *IEEE Transactions on Pattern Analysis and Machine Intelligence* (2025)
25. Liu, Z., Mao, H., Wu, C.Y., Feichtenhofer, C., Darrell, T., Xie, S.: A ConvNet for the 2020s. In: Proceedings of the IEEE/CVF conference on computer vision and pattern recognition. pp. 11976–11986 (2022)
26. Nguyen, V.N., Groueix, T., Salzmann, M., Lepetit, V.: GigaPose: Fast and robust novel object pose estimation via one correspondence. In: Proceedings of the IEEE/CVF Conference on Computer Vision and Pattern Recognition. pp. 9903–9913 (2024)
27. Paul, S., Rao, K., Coviello, G., Sankaradas, M., Po, O., Hu, Y.C., Chakradhar, S.: Enhancing video analytics accuracy via real-time automated camera parameter tuning. In: Proceedings of the 20th ACM Conference on Embedded Networked Sensor Systems. pp. 291–304 (2022)

28. Ponimatkin, G., Cifka, M., Souček, T., Fourmy, M., Labbé, Y., Petrik, V., Sivic, J.: 6D object pose tracking in internet videos for robotic manipulation. In: The Thirteenth International Conference on Learning Representations (2025)
29. Su, Y., Saleh, M., Fetzner, T., Rambach, J., Navab, N., Busam, B., Stricker, D., Tombari, F.: ZebraPose: Coarse to fine surface encoding for 6DoF object pose estimation. In: Proceedings of the IEEE/CVF Conference on Computer Vision and Pattern Recognition. pp. 6738–6748 (2022)
30. Trojak, M., Jurgas, A., Stanuch, M., Kownacki, L., Skalski, A.: Mixed reality 6D object pose estimation using deep learning for visual markerless surgical navigation. In: 2025 IEEE Conference on Virtual Reality and 3D User Interfaces Abstracts and Workshops (VRW). pp. 947–952. IEEE (2025)
31. Tyree, S., Tremblay, J., To, T., Cheng, J., Mosier, T., Smith, J., Birchfield, S.: 6-DoF pose estimation of household objects for robotic manipulation: An accessible dataset and benchmark. In: 2022 IEEE/RSJ International Conference on Intelligent Robots and Systems (IROS). pp. 13081–13088. IEEE (2022)
32. Wang, G., Manhardt, F., Tombari, F., Ji, X.: GDR-Net: Geometry-guided direct regression network for monocular 6D object pose estimation. In: Proceedings of the IEEE/CVF conference on computer vision and pattern recognition. pp. 16611–16621 (2021)
33. Wen, B., Yang, W., Kautz, J., Birchfield, S.: FoundationPose: Unified 6D pose estimation and tracking of novel objects. In: Proceedings of the IEEE/CVF conference on computer vision and pattern recognition. pp. 17868–17879 (2024)
34. Wu, D., Zhuang, Z., Xiang, C., Zou, W., Li, X.: 6D-VNet: End-to-end 6DoF vehicle pose estimation from monocular RGB images. In: Proceedings of the IEEE/CVF Conference on Computer Vision and Pattern Recognition Workshops. pp. 0–0 (2019)
35. Xiang, Y., Schmidt, T., Narayanan, V., Fox, D.: PoseCNN: A convolutional neural network for 6D object pose estimation in cluttered scenes. arXiv preprint arXiv:1711.00199 (2017)
36. Zhang, C., Lin, C., Leng, Y., Fu, Z., Cheng, Y., Fu, C.: An effective head-based HRI for 6D robotic grasping using mixed reality. *IEEE Robotics and Automation Letters* **8**(5), 2796–2803 (2023)
37. Zhao, X., Ding, W., An, Y., Du, Y., Yu, T., Li, M., Tang, M., Wang, J.: Fast segment anything. arXiv preprint arXiv:2306.12156 (2023)

Appendix

A RGB Augmentation Settings

To improve generalization under varying environmental conditions, we adopted an RGB augmentation pipeline based on that used in GDRNPP. The augmentations were implemented using the `imgaug` library and applied only to the RGB input during training with a probability of 0.8. An overview of these augmentations is illustrated in Fig. 6.

The augmentations listed in Tab. 8 were applied in random order, with each operation activated independently with a fixed probability.

Table 8: Augmentation operations and parameters.

Augmentation Type	Activation Probability	Parameters / Range
Gaussian Blur	0.4	$\sigma \in [0.0, 3.0]$
Sharpness Enhancement	0.3	factor $\in [0.0, 50.0]$
Contrast Enhancement	0.3	factor $\in [0.2, 50.0]$
Brightness Enhancement	0.5	factor $\in [0.1, 6.0]$
Color Enhancement	0.3	factor $\in [0.0, 20.0]$
Additive Intensity	0.5	value $\in [-25, 25]$, per-channel = 0.3
Invert Pixels	0.3	probability = 0.2, per-channel
Multiply Intensity	0.5	factor $\in [0.6, 1.4]$, per-channel = 0.5
Additive Gaussian Noise	0.1	scale = 10, per-channel
Linear Contrast	0.5	factor $\in [0.5, 2.2]$, per-channel = 0.3
Grayscale Conversion	0.5	$\alpha \in [0.0, 1.0]$

B Experimental Details

B.1 Computing Resources

All models were trained on a high-performance computing cluster equipped with NVIDIA GPUs and Intel Xeon CPUs. Specifically, *ZebraPose* and *GDRNPP* were trained on nodes with RTX 3090 GPUs (24GB VRAM) and Intel Xeon Silver 4210R CPUs, while *HiPose* was trained on a node with A100 GPUs (80GB VRAM) and an Intel Xeon Gold 6530 CPU. Each training node had access to 512GB of RAM.

B.2 Pretrained Weights for Unseen Object Pose Estimation Models

For GigaPose, we used the pretrained weight files ‘gigaPose_v1’ (coarse) and ‘refiner-rgbd-288182519’ (refiner), following instructions from GigaPose GitHub repository.

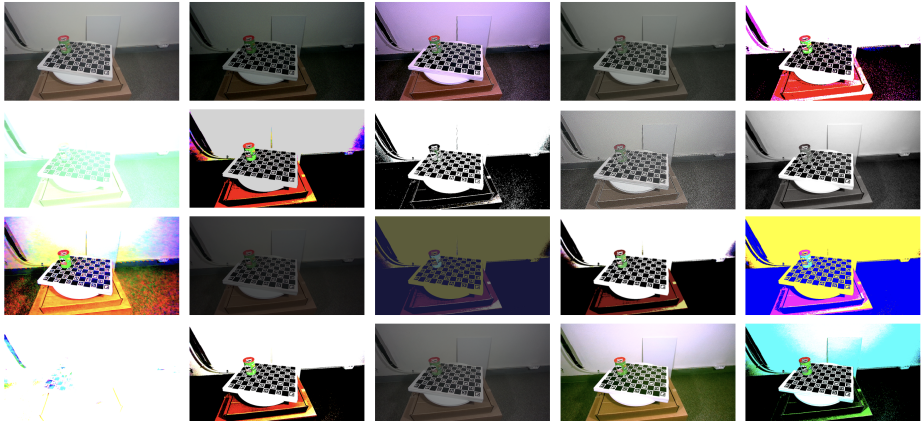


Fig. 6: Examples of RGB augmentations applied during training. The top-left image is the original, and the remaining images are randomly augmented samples generated using the settings summarized in Tab. 8.

For FoundationPose, we used the pretrained weight files ‘2023-10-28-18-33-37’ (refiner) and ‘2024-01-11-20-02-45’ (scorer), following instructions from FoundationPose GitHub repository.

For SAM-6D, we used the pretrained weight file ‘vit_h’ for SAM and the ‘sam-6d-pem-base.pth’ file for the Pose Estimation Module (PEM), following instructions from SAM-6D Github repository.

B.3 Model Training for Instance-Level Pose Estimation Models

All models were trained with a batch size of 32. *ZebraPose* and *HiPose* were both trained for a total of 38,000 iterations using the Adam optimizer, with learning rates of 0.0002 and 0.0001, respectively. *GDRNPP* was trained for 120 epochs using the Ranger optimizer with a learning rate of $8e-4$ and weight decay of 0.01. A flat-and-anneal learning rate schedule with cosine annealing was applied, starting at 72% of the total training epochs. A linear warmup was used for the first 1,000 iterations with a warmup factor of 0.001. All learning rate schedules and optimizer settings follow the original implementations of each method.

C Evaluation of the full SAM-6D pipeline

Tab. 9 presents SAM-6D performance based on the Top-30 segmentation results produced by its ISM.

Table 9: AUC@[0:0.1] performance of SAM-6D with its Image Segmentation Model (ISM).

Object	Baseline	Depth-Only	RGB-Only	Oracle-Fixed	Oracle-Dynamic
	RGB: Auto Depth: Default	RGB: Auto Depth: Oracle	RGB: Oracle Depth: Default	Best Fixed Param.	RGB: Oracle Depth: Oracle
Spray	81.17	86.05 (+4.89)	86.84 (+5.67)	78.71 (-2.46)	89.06 (+7.89)
Pringles	61.84	71.98 (+10.13)	73.80 (+11.96)	55.85 (-6.00)	80.01 (+18.17)
Tincase	63.85	75.66 (+11.81)	75.59 (+11.74)	70.22 (+6.37)	81.71 (+17.86)
Sandwich	74.66	75.44 (+0.78)	80.03 (+5.37)	75.81 (+1.16)	80.85 (+6.19)
Mouse	49.16	55.76 (+6.60)	64.02 (+14.86)	53.48 (+4.32)	68.91 (+19.75)
Duck	74.77	81.31 (+6.53)	82.22 (+7.45)	78.31 (+3.54)	87.01 (+12.24)
Overall	67.57	74.37 (+6.79)	77.08 (+9.51)	68.73 (+1.15)	81.26 (+13.68)

D Evaluation on BOP metrics

Tabs. 10 and 11 report the evaluation using BOP metrics (VSD, MMSD, and MSPD) for pretrained object pose estimation models—GigaPose, SAM-6D, and FoundationPose—and HiPose.

Table 10: Average Recall of VSD, MSSD, and MSPD on various sensor control methods for unseen object pose estimation models: GigaPose, SAM-6D, FoundationPose.

Model	Object	Baseline			Depth-Only			RGB-Only			Oracle-Fixed			Oracle-Dynamic		
		RGB: Auto	Depth: Default	Depth: Oracle	RGB: Auto	Depth: Oracle	Depth: Default	RGB: Oracle	Depth: Default	Best Fixed Param.	Best Fixed Param.	Depth: Oracle	RGB: Oracle	Depth: Oracle		
GigaPose [26]	Spray	71.42	82.68	84.15	84.46	88.68	90.39	83.19	94.05	94.54	77.76	86.15	87.71	91.44	95.22	96.20
	Pringles	79.30	68.24	84.29	88.88	83.14	95.33	93.55	87.90	95.10	84.03	75.76	90.00	97.72	96.05	99.43
	Tincase	85.04	95.87	99.20	90.87	99.16	99.96	90.72	97.16	99.60	86.87	94.93	97.38	96.48	99.60	100.0
	Sandwich	80.50	83.28	86.15	88.76	87.54	87.69	91.89	96.31	99.18	85.12	85.64	86.36	98.21	99.95	100.0
	Mouse	80.26	84.44	94.34	88.41	91.02	96.44	86.94	91.90	98.34	79.34	79.76	88.34	93.90	96.78	99.61
	Duck	92.91	95.77	98.56	97.30	98.74	100.0	95.27	98.23	99.49	94.83	95.86	99.53	98.48	99.44	100.0
Overall		81.57	85.05	91.11	89.78	91.38	94.97	90.26	94.26	97.71	84.66	86.35	91.55	96.04	97.84	99.21
SAM-6D [21]	Spray	92.47	96.33	96.53	94.96	98.00	98.15	91.00	93.66	93.66	92.77	96.33	96.53	97.43	99.22	99.17
	Pringles	94.38	93.08	98.56	97.05	97.76	100.0	95.96	96.57	98.57	94.32	92.43	96.81	99.16	99.62	100.0
	Tincase	97.21	88.08	88.90	96.09	91.91	92.67	95.87	94.22	94.84	96.77	82.60	84.38	97.24	96.76	97.56
	Sandwich	88.74	94.87	94.87	89.42	94.87	94.92	90.19	94.87	95.38	88.65	94.87	94.87	91.32	95.44	96.31
	Mouse	78.79	79.49	85.10	82.08	84.41	89.12	84.92	87.06	91.42	79.04	81.56	86.87	88.56	89.85	93.92
	Duck	93.30	94.88	96.65	96.01	97.12	97.86	97.20	98.56	99.16	94.67	96.37	98.14	98.71	99.07	99.53
Overall		90.82	91.12	93.44	92.60	94.01	95.45	92.52	94.16	95.51	91.03	90.69	92.93	95.40	96.66	97.75
FoundationPose [33]	Spray	89.45	99.22	99.32	92.85	99.76	99.85	94.27	100.0	100.0	89.49	99.32	99.37	97.15	100.0	100.0
	Pringles	93.98	58.29	75.29	96.16	77.00	86.38	96.41	81.10	89.52	94.14	62.43	77.38	99.12	96.10	98.33
	Tincase	97.41	43.11	47.51	97.64	62.62	64.98	97.72	77.73	80.58	97.00	45.33	47.69	97.75	91.47	93.33
	Sandwich	94.49	95.08	96.31	97.26	97.59	98.97	95.75	96.26	98.26	95.87	97.38	97.85	97.96	98.41	99.49
	Mouse	88.39	90.59	94.73	91.24	92.59	97.66	90.72	91.95	96.68	89.02	91.56	96.54	93.66	94.15	98.44
	Duck	98.63	99.42	100.0	99.41	99.63	100.0	99.85	99.95	100.0	98.64	99.57	100.0	99.97	100.0	100.0
Overall		93.72	80.95	85.53	95.76	88.20	91.31	95.79	91.16	94.17	94.03	82.60	86.47	97.60	96.69	98.27

Table 11: Average Recall of VSD, MSSD, and MSPD on various sensor control methods for HiPose.

Object	Baseline		Depth-Only		RGB-Only		Oracle-Fixed		Oracle-Dynamic	
	RGB: Auto	Depth: Default	RGB: Auto	Depth: Oracle	RGB: Oracle	Depth: Default	Best Fixed Param.	RGB: Oracle	Depth: Oracle	
Spray	94.63/99.46	99.56/96.76	99.56/99.61	97.51/99.90	99.95/78.06	82.39/82.39	99.05/99.95	100.0		
Pringles	98.10/96.71	100.0/98.94	97.90/100.0	99.67/99.33	100.0/85.22	84.67/88.38	99.82/99.76	100.0		
Tincase	89.26/88.27	90.67/91.65	90.62/92.76	97.26/97.33	98.44/78.14	78.22/78.98	97.38/97.38	98.84		
Sandwich	92.17/92.77	93.28/94.62	95.23/95.54	95.49/95.74	96.82/76.65	77.69/78.21	97.06/97.38	98.31		
Mouse	79.08/82.98	88.39/82.08	84.98/91.32	86.98/89.46	94.98/65.81	68.98/73.90	90.93/92.73	97.46		
Duck	80.92/81.86	83.07/82.99	83.86/84.84	98.71/99.40	99.77/77.23	78.28/79.35	99.31/99.53	99.86		
Overall	89.03/90.34	92.49/91.17	92.03/94.01	95.94/96.86	98.33/76.85	78.37/80.20	97.26/97.79	99.08		

E Evaluation on Markerless Test Scenes

Since visible markers in the scene can introduce model bias [10], we modified Test-Var split images (see Fig. 7) and evaluated them using (i) the same model weights as in Sec. 4.2 (Tab. 12) and (ii) models trained on the PBR + marker-removed Train-Def setting (Tab. 13).



Fig. 7: Sample of marker-removed test images.

In Tab. 12, the RGB-D based model (i.e., HiPose [22]) maintains performance comparable to Tab. 5, whereas the RGB-based models (i.e., ZebraPose [29] and GDRNPP [24]) show substantial object-dependent variation. Both RGB models retain similar performance for Spray compared to Tab. 5, but exhibit a dramatic drop for Mouse. Meanwhile, Tab. 13 shows overall performance comparable to Tab. 5. These results suggest that Spray, which has rich RGB features, can be learned based on its distinctive texture. In contrast, Mouse, which has an ambiguous shape and pale coloration, lacks discriminative features, making the models more susceptible to domain shift. Despite these discrepancies, sensor optimization consistently adapts to environmental changes more effectively than existing generalization techniques, even without additional training.

Table 12: AR@5 comparison of sensor control methods on marker-removed *SenseShift6D* with ZebraPose, GDRNPP, and HiPose.

Object	Train	ZebraPose [29]			GDRNPP [24]			HiPose [22]					
		Test-Def		Test-Var	Test-Def		Test-Var	Test-Def		Test-Var			
		Auto	Auto Rand Oracle	Auto	Auto Rand Oracle	Auto	Auto Rand Oracle						
Spray	PBR + Train-Def	96.59	95.12	64.33	100	100	96.59	52.49	99.51	100	98.73	59.98	100
	PBR + Train-Def w/ Aug	93.66	93.17	70.71	100	95.12	94.63	71.63	100	100	100	91.66	100
	PBR + Train-Var	98.05	97.07	78.91	100	100	100	81.89	100	100	100	100	100
Tincase	PBR + Train-Def	94.22	86.22	55.45	99.11	64.44	58.66	35.07	84.89	97.78	84.62	56.33	97.78
	PBR + Train-Def w/ Aug	76.44	72.89	52.62	87.11	40	38.22	26.69	61.33	97.78	96.89	88.40	97.78
	PBR + Train-Var	85.33	81.33	59.79	96.00	51.11	48.44	34.40	71.56	97.78	97.69	97.73	97.78
Mouse	PBR + Train-Def	48.78	43.41	30.63	84.88	4.88	3.90	2.98	29.27	90.24	67.42	47.17	88.78
	PBR + Train-Def w/ Aug	26.83	24.39	18.83	57.56	12.2	12.17	11.66	45.37	90.24	88.49	84.56	90.24
	PBR + Train-Var	9.76	8.29	5.07	25.37	2.44	1.95	3.39	19.02	90.24	90.15	87.68	90.73

Table 13: AR@5 comparison of sensor control methods on marker-removed *SenseShift6D* with ZebraPose, GDRNPP, and HiPose trained on PBR + marker-removed Train-Def setting.

		ZebraPose [29]				GDRNPP [24]				HiPose [22]			
		Test-Def		Test-Var		Test-Def		Test-Var		Test-Def		Test-Var	
Object	Train	Auto	Auto Rand	Oracle	Auto	Auto Rand	Oracle	Auto	Auto Rand	Oracle	Auto	Auto Rand	Oracle
Spray	PBR + Train-Def	100.0	97.56	55.95	99.51	100.0	95.12	50.76	98.54	100.0	97.07	56.49	100.0
	PBR + Train-Def w/ Aug	97.56	89.78	66.95	100.00	97.56	97.07	76.10	99.51	100.0	100.0	98.71	100.0
	PBR + Train-Var	95.12	90.73	73.85	97.56	95.12	95.12	87.61	95.12	100.0	100.0	99.73	100.0
Tincase	PBR + Train-Def	97.78	96.10	50.89	98.67	93.33	82.22	47.60	94.67	97.33	82.49	53.82	96.44
	PBR + Train-Def w/ Aug	97.78	92.00	64.82	100.0	91.11	87.55	66.51	95.56	97.78	95.82	77.20	97.78
	PBR + Train-Var	95.56	95.56	82.09	97.78	100.0	99.56	93.16	100.0	97.78	97.78	97.73	97.78
Mouse	PBR + Train-Def	75.61	65.85	27.59	92.68	90.24	75.12	32.07	88.29	85.85	70.54	45.61	89.27
	PBR + Train-Def w/ Aug	51.22	56.59	46.46	94.63	73.17	68.78	47.93	88.78	90.24	89.56	73.17	90.24
	PBR + Train-Var	58.54	56.59	48.37	79.51	73.17	73.66	69.02	85.85	90.24	90.05	89.17	90.73

F Qualitative Analysis

F.1 Qualitative Result on Pretrained, Generalizable Pose Estimation Models

Fig. 8, Fig. 9, Fig. 10 visualize GT and predicted poses on Baseline and Oracle sensor configuration for GigaPose, SAM-6D and FoundationPose.

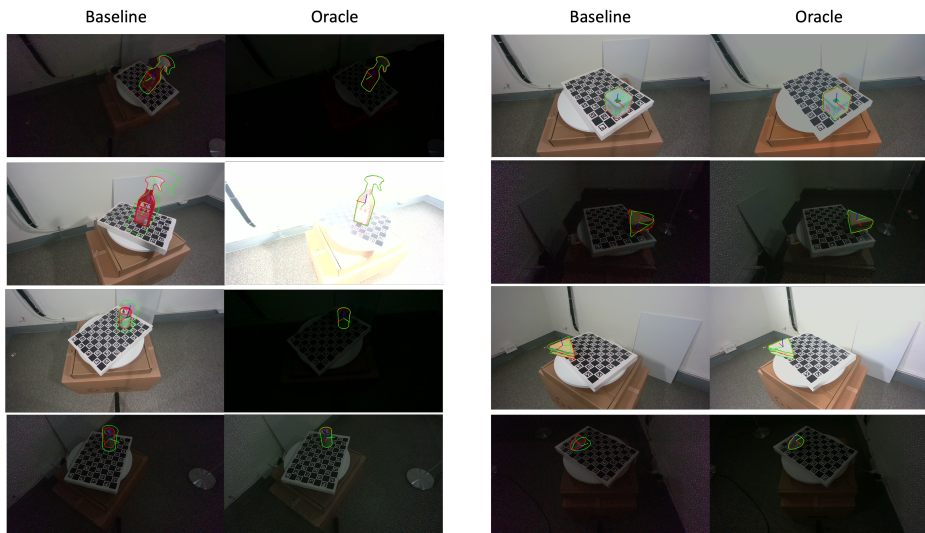


Fig. 8: Comparison of predictions under Baseline and Oracle for GigaPose. Visualized object pose on RGB images: ground truth pose in red, predicted pose in green.



Fig. 9: Comparison of predictions under Baseline and Oracle for SAM-6D. Visualized object pose on RGB images: ground truth pose in red, predicted pose in green.

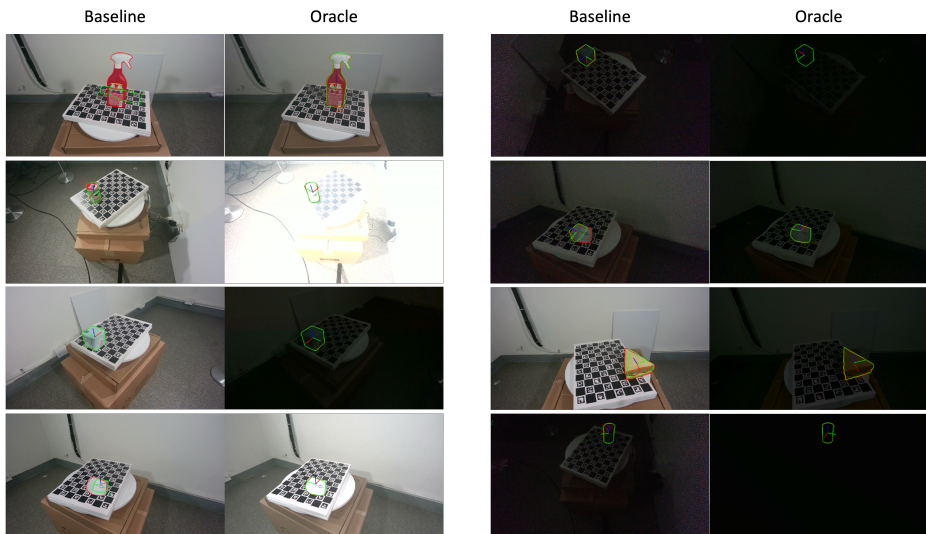


Fig. 10: Comparison of predictions under Baseline and Oracle for FoundationPose. Visualized object pose on RGB images: ground truth pose in red, predicted pose in green.

F.2 Qualitative Result on Instance-Level Pose Estimation Model

Fig. 11 visualizes GT and predicted poses on Baseline and Oracle sensor configuration for HiPose.

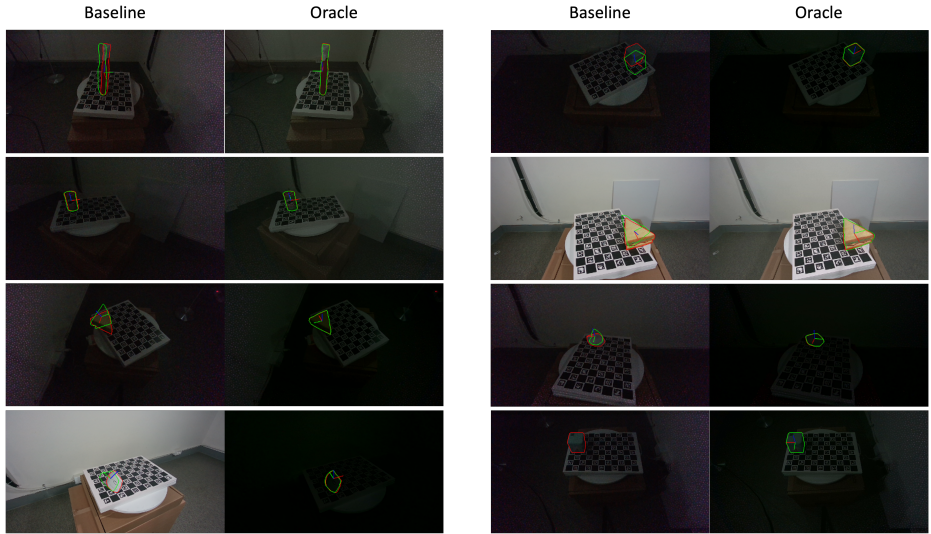


Fig. 11: Comparison of predictions under Baseline and Oracle for HiPose. Visualized object pose on RGB images: ground truth pose in red, predicted pose in green.

G Evaluation on RGB-D Based Models Under Different Environments

Tab. 14, Tab. 15, Tab. 16, Tab. 17 shows performance of RGB-D models—HiPose, GigaPose, SAM-6D, and FoundationPose—under different illumination conditions.

Table 16: AUC@[0:0.1] performance under diverse environments of various sensor control methods for SAM-6D.

Env	Object	Baseline	Depth-Only	RGB-Only	Oracle-Fixed	Oracle-Dynamic
		RGB: Auto Depth: Default	RGB: Auto Depth: Oracle	RGB: Oracle Depth: Default	Best Fixed Param.	RGB: Oracle Depth: Oracle
B5	Spray	84.54	86.83 (+2.29)	84.22 (-0.32)	86.59 (+2.05)	89.22 (+4.68)
	Pringles	50.17	71.45 (+21.28)	69.14 (+18.97)	65.76 (15.59)	80.48 (+30.31)
	Tincase	47.61	66.73 (+19.12)	77.96 (+30.34)	68.61 (+21.00)	80.67 (+33.05)
	Sandwich	78.36	79.00 (+0.64)	80.10 (+1.74)	78.41 (+0.05)	80.85 (+2.49)
	Mouse	52.41	64.83 (+12.41)	69.12 (+16.71)	59.54 (+7.13)	74.40 (+21.99)
	Duck	76.93	81.42 (+4.49)	84.56 (+7.63)	79.21 (+2.28)	87.91 (10.98)
	Overall	65.00	75.04 (+10.04)	77.52 (+12.51)	73.02 (+8.02)	82.25 (+17.25)
B25	Spray	82.00	85.90 (+3.90)	77.80 (-4.20)	82.68 (+0.68)	89.49 (+7.49)
	Pringles	65.85	73.93 (+8.07)	72.90 (7.05)	66.95 (+1.10)	80.67 (+14.81)
	Tincase	79.66	80.71 (+1.05)	81.62 (+1.96)	79.86 (+0.20)	84.64 (+4.99)
	Sandwich	78.10	78.74 (+0.64)	80.10 (+2.00)	78.44 (+0.33)	80.85 (+2.74)
	Mouse	55.90	62.59 (+6.69)	66.90 (+11.00)	62.50 (+6.60)	72.32 (+16.42)
	Duck	75.65	82.40 (+6.74)	82.74 (+7.09)	79.07 (+3.42)	87.47 (+11.81)
	Overall	72.86	77.38 (+4.52)	77.01 (+4.15)	74.92 (+2.06)	82.57 (+9.71)
B50	Spray	80.56	84.29 (+3.73)	81.93 (+1.36)	84.70 (+4.14)	89.44 (+8.87)
	Pringles	67.45	74.74 (+7.29)	75.95 (+8.50)	71.26 (+3.81)	81.31 (+13.86)
	Tincase	80.00	80.58 (+0.58)	79.76 (-0.24)	78.18 (-1.82)	84.49 (+4.49)
	Sandwich	78.38	79.18 (+0.79)	79.77 (+1.38)	78.59 (+0.21)	80.69 (+2.31)
	Mouse	56.35	62.76 (+6.41)	66.90 (+10.55)	59.80 (+3.45)	71.68 (+15.33)
	Duck	77.21	82.60 (+5.40)	83.23 (+6.02)	80.02 (+2.81)	87.70 (+10.49)
	Overall	73.33	77.36 (+4.03)	77.92 (+4.60)	75.43 (+2.10)	82.55 (+9.22)
B75	Spray	82.85	85.88 (+3.03)	83.76 (+0.91)	86.47 (+3.62)	87.17 (+4.32)
	Pringles	67.48	75.38 (+7.90)	76.62 (+9.14)	70.45 (+2.98)	80.29 (+12.81)
	Tincase	81.14	80.69 (-0.45)	82.87 (+1.73)	81.18 (+0.05)	84.18 (+3.04)
	Sandwich	78.38	78.77 (+0.38)	80.00 (+1.62)	78.97 (+0.59)	80.72 (+2.33)
	Mouse	56.69	59.54 (+2.84)	67.41 (+10.72)	63.05 (+6.36)	71.37 (+14.67)
	Duck	75.72	83.00 (+7.28)	83.60 (+7.88)	79.86 (+4.14)	88.21 (+12.49)
	Overall	73.71	77.21 (+3.50)	79.04 (+5.33)	76.67 (+2.96)	81.99 (+8.28)
B100	Spray	85.67	85.20 (-0.48)	85.49 (-0.19)	86.12 (+0.45)	87.20 (+1.52)
	Pringles	69.21	74.31 (+5.10)	75.74 (+6.52)	71.07 (+1.86)	80.40 (+11.19)
	Tincase	78.79	78.93 (+0.14)	78.73 (-0.06)	80.77 (+1.98)	82.60 (+3.81)
	Sandwich	78.74	79.28 (+0.54)	80.13 (+1.38)	79.55 (+0.81)	80.92 (+2.18)
	Mouse	57.20	61.61 (+4.41)	68.12 (+10.92)	61.47 (+4.27)	72.51 (+15.31)
	Duck	77.86	82.67 (+4.81)	82.84 (+4.98)	80.93 (+3.07)	86.93 (+9.07)
	Overall	74.58	77.00 (+2.42)	78.51 (+3.93)	76.65 (+2.07)	81.76 (+7.18)

Table 14: AUC@[0:0.1] performance under diverse environments of various sensor control methods for HiPose trained on PBR + Train-Def.

Env	Object	Baseline	Depth-Only	RGB-Only	Oracle-Fixed	Oracle-Dynamic
		RGB: Auto Depth: Default	RGB: Auto Depth: Oracle	RGB: Oracle Depth: Default	Best Fixed Param.	RGB: Oracle Depth: Oracle
B5	Spray	83.17	85.07 (+1.90)	87.10 (+3.93)	86.07 (+2.90)	88.63 (+5.46)
	Pringles	72.40	75.45 (+3.05)	78.60 (+6.19)	77.90 (+5.50)	81.12 (+8.71)
	Tincase	32.96	43.00 (+10.04)	78.80 (+45.84)	76.69 (+43.73)	81.31 (+48.36)
	Sandwich	66.85	69.85 (+3.00)	80.72 (+13.87)	78.82 (+11.97)	83.18 (+16.33)
	Mouse	35.29	39.88 (+4.59)	64.85 (+29.56)	62.93 (+27.63)	69.88 (+34.59)
	Duck	5.93	12.05 (+6.12)	79.16 (+73.23)	76.14 (+70.21)	81.44 (+75.51)
	Overall	49.43	54.22 (+4.78)	78.20 (+28.77)	76.43 (+26.99)	80.93 (+31.49)
B25	Spray	87.56	88.71 (+1.15)	88.61 (+1.05)	87.59 (+0.02)	89.63 (+2.07)
	Pringles	74.12	77.17 (+3.05)	79.14 (+5.02)	77.31 (+3.19)	81.74 (+8.62)
	Tincase	85.20	86.33 (+1.13)	86.91 (+1.71)	85.13 (-0.07)	87.89 (+2.69)
	Sandwich	80.54	83.51 (+2.97)	83.31 (+2.77)	82.97 (+2.44)	86.51 (+5.97)
	Mouse	70.41	73.17 (+2.76)	74.32 (+3.90)	71.54 (+1.12)	77.29 (+6.88)
	Duck	85.88	86.93 (+1.05)	88.47 (+2.58)	87.16 (+1.28)	90.02 (+4.14)
	Overall	80.62	82.64 (+2.02)	83.46 (+2.84)	81.95 (+1.33)	85.51 (+4.90)
B50	Spray	87.93	88.78 (+0.85)	89.32 (+1.39)	88.07 (+0.15)	90.07 (+2.15)
	Pringles	74.24	76.57 (+2.33)	79.69 (+5.45)	76.74 (+2.50)	81.62 (+7.38)
	Tincase	85.11	86.69 (+1.58)	86.91 (+1.80)	85.29 (+0.18)	88.31 (+3.20)
	Sandwich	81.38	84.38 (+3.00)	85.72 (+4.33)	84.03 (+2.64)	87.23 (+5.85)
	Mouse	71.93	73.17 (+1.24)	74.51 (+2.59)	71.63 (-0.29)	77.44 (+5.51)
	Duck	86.77	88.51 (+1.74)	88.63 (+1.86)	87.51 (+0.74)	90.49 (+3.72)
	Overall	81.23	83.02 (+1.79)	84.13 (+2.90)	82.21 (+0.99)	85.86 (+4.63)
B75	Spray	88.02	89.02 (+1.00)	89.51 (+1.49)	88.02 (+0.00)	90.61 (+2.59)
	Pringles	73.31	76.02 (+2.71)	79.12 (+5.81)	76.83 (+3.52)	81.86 (+8.55)
	Tincase	85.27	86.49 (+1.22)	86.80 (+1.53)	85.33 (+0.07)	88.13 (+2.87)
	Sandwich	82.10	85.13 (+3.03)	84.41 (+2.31)	84.38 (+2.28)	87.10 (+5.00)
	Mouse	71.73	73.27 (+1.54)	74.17 (+2.44)	71.24 (-0.49)	76.07 (+4.34)
	Duck	86.93	88.70 (+1.77)	88.67 (+1.74)	86.35 (-0.58)	89.79 (+2.86)
	Overall	81.23	83.11 (+1.88)	83.78 (+2.55)	82.03 (+0.80)	85.59 (+4.37)
B100	Spray	87.93	89.27 (+1.34)	89.39 (+1.46)	87.95 (+0.02)	90.41 (+2.49)
	Pringles	72.90	75.69 (+2.79)	78.86 (+5.95)	76.31 (+3.40)	81.40 (+8.50)
	Tincase	85.38	86.87 (+1.49)	87.09 (+1.71)	85.40 (+0.02)	88.53 (+3.16)
	Sandwich	82.51	85.72 (+3.21)	86.15 (+3.64)	84.31 (+1.80)	88.10 (+5.59)
	Mouse	70.24	72.59 (+2.34)	73.07 (+2.83)	70.24 (+0.00)	75.39 (+5.15)
	Duck	85.86	88.53 (+2.67)	88.44 (+2.58)	87.12 (+1.26)	90.56 (+4.70)
	Overall	80.80	83.11 (+2.31)	83.83 (+3.03)	81.89 (+1.08)	85.73 (+4.93)

Table 15: AUC@[0:0.1] performance under diverse environments of various sensor control methods for GigaPose.

Env	Object	Baseline	Depth-Only	RGB-Only	Oracle-Fixed Best Fixed Param.	Oracle-Dynamic
		RGB: Auto Depth: Default	RGB: Auto Depth: Oracle	RGB: Oracle Depth: Default		RGB: Oracle Depth: Oracle
B5	Spray	65.76	73.34 (+7.58)	73.39 (+7.63)	66.51 (+0.75)	78.41 (+12.65)
	Pringles	19.17	44.19 (+25.02)	44.64 (+25.47)	31.33 (+12.16)	66.69 (+47.52)
	Tincase	60.69	71.51 (+10.82)	65.20 (+4.51)	65.89 (+5.20)	75.07 (+14.38)
	Sandwich	59.90	68.82 (+8.92)	69.46 (+9.56)	61.36 (+1.46)	80.28 (+20.38)
	Mouse	48.27	60.44 (+12.17)	63.80 (+15.53)	55.59 (+7.32)	74.29 (+26.02)
	Duck	73.12	77.07 (+3.95)	75.95 (+2.84)	72.70 (-0.42)	80.70 (+7.58)
	Overall	54.48	65.90 (+11.41)	65.41 (+10.93)	58.90 (+4.41)	75.91 (+21.43)
B25	Spray	67.44	73.20 (+5.76)	77.78 (+10.34)	70.49 (+3.05)	81.15 (+13.71)
	Pringles	15.62	49.24 (+33.62)	49.36 (+33.74)	38.17 (+22.55)	73.88 (+58.26)
	Tincase	63.07	72.13 (+9.06)	69.29 (+6.22)	67.29 (+4.22)	75.69 (+12.62)
	Sandwich	68.08	74.18 (+6.10)	77.72 (+9.64)	75.79 (+7.71)	84.59 (+16.51)
	Mouse	61.93	69.71 (+7.78)	68.15 (+6.22)	61.95 (+0.02)	77.00 (+15.07)
	Duck	71.35	78.56 (+7.21)	77.07 (+5.72)	74.58 (+3.23)	82.30 (+10.95)
	Overall	57.91	69.50 (+11.59)	69.89 (+11.98)	64.71 (+6.80)	79.10 (+21.19)
B50	Spray	65.51	73.71 (+8.20)	77.20 (+11.69)	71.10 (+5.59)	83.78 (+18.27)
	Pringles	24.43	45.40 (+20.97)	43.33 (+18.90)	33.50 (+9.07)	70.14 (+45.71)
	Tincase	64.98	72.42 (+7.44)	70.22 (+5.24)	68.31 (+3.33)	76.82 (+11.84)
	Sandwich	63.92	70.46 (+6.54)	77.51 (+13.59)	78.03 (+14.11)	84.38 (+20.46)
	Mouse	56.93	68.93 (+12.00)	67.98 (+11.05)	63.68 (+6.75)	78.20 (+21.27)
	Duck	72.07	79.19 (+7.12)	79.44 (+7.37)	76.12 (+4.05)	83.09 (+11.02)
	Overall	57.97	68.35 (+10.38)	69.28 (+11.31)	65.12 (+7.15)	79.40 (+21.43)
B75	Spray	61.41	71.10 (+9.69)	77.37 (+15.96)	70.68 (+9.27)	81.41 (+20.00)
	Pringles	22.88	47.57 (+24.69)	45.69 (+22.81)	35.12 (+12.24)	72.00 (+49.12)
	Tincase	66.78	73.36 (+6.58)	71.49 (+4.71)	70.78 (+4.00)	77.36 (+10.58)
	Sandwich	66.72	73.00 (+6.28)	77.79 (+11.07)	78.44 (+11.72)	84.95 (+18.23)
	Mouse	55.59	68.66 (+13.07)	67.63 (+12.04)	63.61 (+8.02)	76.93 (+21.34)
	Duck	72.98	79.14 (+6.16)	78.47 (+5.49)	76.09 (+3.12)	83.51 (+10.53)
	Overall	57.73	68.80 (+11.08)	69.74 (+12.01)	65.79 (+8.06)	79.36 (+21.63)
B100	Spray	59.59	70.71 (+11.12)	76.37 (+16.78)	70.71 (+11.12)	81.44 (+21.85)
	Pringles	22.48	47.31 (+24.83)	47.64 (+25.16)	33.12 (+10.64)	70.00 (+47.52)
	Tincase	66.93	73.91 (+6.98)	70.42 (+3.49)	69.38 (+2.45)	77.13 (+10.20)
	Sandwich	66.10	73.15 (+7.05)	77.95 (+11.85)	76.77 (+10.67)	85.21 (+19.11)
	Mouse	60.39	69.29 (+8.90)	67.54 (+7.15)	63.12 (+2.73)	77.15 (+16.76)
	Duck	71.79	79.63 (+7.84)	77.40 (+5.60)	75.47 (+3.67)	83.51 (+11.72)
	Overall	57.88	69.00 (+11.12)	69.55 (+11.67)	64.76 (+6.88)	79.07 (+21.19)

Table 17: AUC@[0:0.1] performance under diverse environments of various sensor control methods for FoundationPose.

Env	Object	Baseline	Depth-Only	RGB-Only	Oracle-Fixed	Oracle-Dynamic
		RGB: Auto Depth: Default	RGB: Auto Depth: Oracle	RGB: Oracle Depth: Default	Best Fixed Param.	RGB: Oracle Depth: Oracle
B5	Spray	82.80	84.68 (+1.88)	85.34 (+2.54)	83.44 (+0.64)	87.17 (+4.37)
	Pringles	25.07	39.45 (+14.38)	45.26 (+20.19)	32.98 (+7.91)	64.10 (+39.03)
	Tincase	26.47	49.11 (+22.64)	53.64 (27.18)	38.29 (+11.82)	74.24 (+47.78)
	Sandwich	81.62	84.41 (+2.79)	83.38 (+1.76)	82.77 (+1.15)	86.28 (+4.66)
	Mouse	67.88	72.80 (+4.92)	75.10 (+7.22)	72.02 (+4.14)	79.54 (+11.66)
	Duck	82.58	85.21 (+2.63)	87.88 (+5.30)	84.07 (+1.49)	89.74 (+7.16)
	Overall	61.07	69.28 (+8.21)	71.77 (+10.70)	65.59 (+4.52)	80.18 (+19.11)
B25	Spray	84.85	86.37 (+1.52)	87.17 (+2.32)	84.90 (+0.05)	88.46 (+3.61)
	Pringles	40.24	51.57 (+11.33)	51.36 (+11.12)	44.67 (+4.43)	71.07 (+30.83)
	Tincase	37.91	54.42 (+16.51)	65.98 (+28.07)	50.93 (+13.02)	80.00 (+42.09)
	Sandwich	83.36	86.72 (+3.36)	84.90 (+1.54)	84.10 (+0.74)	87.97 (+4.61)
	Mouse	71.39	75.37 (+3.98)	75.98 (+4.59)	72.66 (+1.27)	80.51 (+9.12)
	Duck	84.74	87.16 (+2.42)	88.65 (+3.91)	85.63 (+0.88)	90.40 (+5.65)
	Overall	67.08	73.60 (+6.52)	75.67 (+8.59)	70.48 (+3.40)	83.07 (+15.99)
B50	Spray	85.49	86.85 (+1.36)	88.22 (+2.73)	85.32 (-0.17)	89.59 (+4.10)
	Pringles	35.67	55.31 (+19.64)	50.74 (+15.07)	45.50 (+9.83)	79.00 (+43.33)
	Tincase	45.60	60.09 (+14.49)	75.58 (+29.98)	56.64 (+11.04)	85.00 (+39.40)
	Sandwich	83.62	87.13 (+3.51)	85.46 (+1.84)	85.00 (+1.38)	88.56 (+4.94)
	Mouse	70.71	74.39 (+3.68)	75.78 (+5.07)	72.51 (+1.80)	79.88 (+9.17)
	Duck	85.23	87.33 (+2.09)	90.19 (+4.95)	85.74 (+0.51)	91.42 (+6.19)
	Overall	67.72	75.18 (+7.46)	77.66 (+9.94)	71.79 (+4.07)	85.57 (+17.86)
B75	Spray	85.93	87.20 (+1.27)	88.73 (+2.80)	86.12 (+0.19)	89.83 (+3.90)
	Pringles	35.19	49.95 (+14.76)	60.00 (+24.81)	54.76 (+19.57)	81.88 (+46.69)
	Tincase	41.87	58.62 (+16.76)	75.73 (+33.87)	55.31 (+13.44)	87.27 (+45.40)
	Sandwich	83.56	86.82 (+3.26)	85.82 (+2.26)	84.92 (+1.36)	88.92 (+5.36)
	Mouse	70.98	74.78 (+3.80)	75.59 (+4.61)	72.88 (+1.90)	80.10 (+9.12)
	Duck	85.79	87.49 (+1.70)	89.95 (+4.16)	85.95 (+0.16)	91.21 (+5.42)
	Overall	67.22	74.14 (+6.92)	79.30 (+12.09)	73.32 (+6.11)	86.53 (+19.32)
B100	Spray	84.07	87.51 (+3.44)	88.54 (+4.47)	86.00 (+1.93)	90.00 (+5.93)
	Pringles	35.14	57.31 (+22.17)	46.55 (+11.41)	48.07 (+12.93)	77.40 (+42.26)
	Tincase	39.36	58.56 (+19.20)	75.96 (+36.60)	55.09 (+15.73)	87.42 (+48.07)
	Sandwich	83.69	86.92 (+3.23)	86.03 (+2.34)	85.21 (+1.52)	88.82 (+5.13)
	Mouse	70.17	74.37 (+4.20)	76.88 (+6.71)	72.46 (+2.29)	79.85 (+9.68)
	Duck	85.16	87.16 (+2.00)	89.09 (+3.93)	85.33 (+0.16)	90.58 (+5.42)
	Overall	66.27	75.30 (+9.04)	77.17 (+10.91)	72.03 (+5.76)	85.68 (+19.41)

H ADD-VSD Correlation

Tab. 18 reports correlation coefficients computed under the experimental settings described in Sec. 4.1 and the PBR+Train-Def scheme of Sec. 4.2. The correlations are first computed at the scene level across all sensor configurations, and then Fisher’s z -transformation is applied before averaging them across scenes.

Table 18: Correlation analysis between ADD and AR_{VSD} . r denotes the Pearson correlation coefficient and ρ_s denotes the Spearman rank correlation coefficient. For pretrained models, correlations are reported for both ADD(-S) and AR_{VSD} .

(a) Supervised Models

ZebraPose [29]		GDRNPP [24]		HiPose [22]	
$ r $	$ \rho_s $	$ r $	$ \rho_s $	$ r $	$ \rho_s $
0.862	0.937	0.945	0.923	0.975	0.920

(b) Pretrained Models.

GigaPose [26]		SAM-6D [21]		FondationPose [33]	
$ r $	$ \rho_s $	$ r $	$ \rho_s $	$ r $	$ \rho_s $
0.813	0.721	0.718	0.715	0.696	0.621
(0.889)	(0.860)	(0.787)	(0.788)	(0.789)	(0.730)